Published in the proceedings of HYDROPOWER INTO THE NEXT CENTURY - III, 1999. ISBN 0 9522642 9 3

A numerical investigation of tip clearance flow in Kaplan water turbines

M.Sc. H. Nilsson
Chalmers University of Technology
Thermo and Fluid Dynamics
S - 412 96 Gothenburg
Sweden
hani@tfd.chalmers.se

Prof. L. Davidson
Chalmers University of Technology
Thermo and Fluid Dynamics
S - 412 96 Gothenburg
Sweden
lada@tfd.chalmers.se

Introduction

A parallel multiblock finite volume CFD (Computational Fluid Dynamics) code CALC-PMB (Parallel MultiBlock) for computations of turbulent flow in complex domains has been developed for an investigation of the turbulent flow in Kaplan water turbines. The main features of the code are the use of general curvilinear coordinates, pressure correction scheme (SIMPLEC [6]), cartesian velocity components as principal unknowns, and collocated grid arrangement together with Rhie and Chow interpolation. The computational blocks are solved in parallel with Dirichlet-Dirichlet coupling using PVM (Parallel Virtual Machine) or MPI (Message Passing Interface). The parallel efficiency is excellent, with super scalar speedup for load balanced applications [3]. For grid generation, the commercial grid generator ICEM CFD/CAE is used and for post-processing the commercial post-processors Tecplot and Ensight are used.

This work is focused on tip clearance losses, which reduces the efficiency of a Kaplan water turbine by about 0.5%. The investigated turbine is a test rig with a runner diameter of $0.5m$. It has four runner blades and 24 guide vanes. The tip clearance between the runner blades and the shroud is $0.25mm$. In order to resolve the turbulent flow in the tip clearance and in the boundary layers, a low Reynolds number $k-\omega$ turbulence model is used. Because of computational restrictions, complete turbine simulations usually use wall functions instead of resolving the boundary layers, which makes tip clearance investigations impossible.

The computational domain starts at the trailing edge of the guide vanes and ends at the inlet of the draft tube in a 90 degree section, including one runner blade, of the investigated Kaplan water turbine. This restricts the flow to being periodic, but reduces the computational domain to 1/4 of the original size and allows stationary calculations. Complete turbine simulations commonly applies a circumferential averaging between the distributor and the runner, yielding the same periodic restriction. In reality the inlet flow is slightly non-periodic and concists of wakes from the guide vanes, which results in varying angles of incidence and require transient calculations. The present work investigates the flow structures for stationary periodic turbulent mean flow comparing different inlet guide vane angles. The runner blade angles are kept at a constant value ($\alpha = 0$) so that the same grid may be used for all cases. The calculations are performed in a rotating coordinate system where Coriolis and centripetal force terms have been added to the momentum equations.

The computational results from four different operating conditions, with different guide vane angles, are compared in this work. It is found that

- The computations capture a vortical structure close to the leading edge tip clearance, where the tip clearance flow interacts with the shroud boundary layer and cavitational bubbles are formed.
- The tip blade loading increases when the specific speed decreases. This is in accordance with with the turbine manufacturer [9].
- The magnitude of the axial flow in the tip clearance, close to the leading edge, increases when the specific speed decreases. This is in accordance with the tip cavitation pattern of the investigated turbine.
- Detailed measurements need to be performed, for use as boundary conditions and validation of the results.
- Transient features of the flow should be studied, using LES (Large Eddy Simulation).

The tip clearance flow pattern is in accordance with observations of the investigated turbine. However, future work will focus on further comparisons of the computational results to measurements. Measurements will also be used to improve the boundary conditions. Transient calculations using LES (Large Eddy Simulation) will be performed in order to capture the effects of the guide vane wakes and the instabilities of the tip vortex.

Case	N_{11} $\left(\frac{ND}{\sqrt{H}}\right)$	Q_{11} $\left(\frac{Q}{D^2\sqrt{H}}\right)$	γ (guide vane angle)	η (efficiency)
k15	160.1	1.195	35.1	92.40
k138	150.0	1.136	33.3	92.62
k150	145.0	1.115	33.0	92.56
k123	140.0	1.084	31.9	92.26

Table 2.1: The operating conditions used in this work.

1 Background

The present work is a part of a Swedish water turbine program, presently involving six Ph.D. students in Göteborg (CTH), Stockholm (KTH), Älvkarleby (Vattenfall Utveckling AB) and Luleå (LUTH). It is financed by a collaboration between the Swedish power industry via ELFORSK (Swedish Electrical Utilities Research and Development Company), the Swedish National Energy Administration and Kvaerner Turbin AB. The purpose of the program is to increase the Swedish water power competence in order to meet the growing water power demand in Sweden together with the demands on environmental care and efficiency. Also, an increased collaboration between industry and universities as well as international collaboration is established.

At Kvaerner Turbin AB, Kaplan turbines with outputs up to 183MW, with runner diameters up to 8.3m and for heads up to 59.5m has been designed, manufactured and installed. Their development of the first large dimension Kaplan turbine in the world started in 1922 and resulted in the unit at Lilla Edet in Sweden with a runner diameter of 5.8m, an output of 8.2MW and a head of 6.5m.

The geometry used in this work originates from the T24 [9] test rig for efficiency and cavitation testing of Kaplan and Bulb turbines at Kvaerner Turbin AB in Kristinehamn, Sweden. Measured quantities in the test rig are rotational speed, volume flow, head and torque. The accuracy of the efficiency measurements are about 0.2%. The model testing is an iterative procedure where the impact of modifications to the model runner is analysed based on the measurements and experience. The results obtained from the model testing is then scaled up to the real size turbine using empirically determined relations. It is very important to capture the final turbine efficiency and the power output at the model testing stage, because of the fines involved when they are not. It is believed that future CFD (Computational Fluid Dynamics) can be a complement to this model testing, speeding up the design procedure. However, the introduction of CFD in production of water turbines cannot be done without experience of CFD comparable to experience of model testing in this field. The purpose of this work is to increase the experience of CFD in the water turbine field.

2 Computational cases

The Kaplan geometry used in this work is the runner part of the model section of the T24 test rig at Kvaerner Turbin AB in Kristinehamn, Sweden. It has four runner blades and 24 guide vanes. The runner diameter is $0.5m$ and the tip clearance is $0.25mm$. The runner clearance at the hub is not included in the calculations and the computational domain starts after the guide vanes, assuming axisymmetric flow defined by the guide vane angle and the volume flow. The computations are performed using the CFD code CALC-PMB (Parallel MultiBlock), which is an extension of the CFD code CALC-BFC (Boundary Fitted Coordinates) [5, 10] for parallel multiblock calculations.

2.1 Operating conditions

The different operating conditions used as test cases in this work is displayed in table 2.1, where N_{11} is the specific speed, Q_{11} is the specific flow, N is the rotational speed, Q is the volume flow, D is the runner diameter, H is the head, γ is the guide vane angle and η is the turbine efficiency. The test case names are used when presenting the results. The runner blade angle is kept constant ($\alpha = 0$) so that the same grid may be used in all cases. Because of this a lot of work is saved and the results may be compared without grid dependence. Even though the efficiency is not largest at $N_{11} = 160.1$, case k15 is decided to be the best point of operation. The reason for this is that other features, such as tip clearance cavitation, become important for the other cases. The main differences between the flow in these cases is that the leading edge load and the tip cavitation increases when N_{11} decreases [9].

2.2 Equations

The equations used for the computations are briefly described below.

The Reynolds time averaged continuity and Navier Stokes equations for incompressible flow in a rotating frame of reference reads [8, 4]

$$\frac{\partial \rho U_i}{\partial x_i} = 0$$

$$\frac{\partial \rho U_i}{\partial t} + \frac{\partial \rho U_i U_j}{\partial x_j} =$$
$$-\frac{\partial P}{\partial x_i} + \frac{\partial}{\partial x_j}\left(\mu\left(\frac{\partial U_i}{\partial x_j} + \frac{\partial U_j}{\partial x_i}\right) - \rho\overline{u_i' u_j'}\right) + \rho g_i - \rho\epsilon_{ijk}\epsilon_{klm}\Omega_j\Omega_l x_m - 2\rho\epsilon_{ijk}\Omega_j U_k$$

where $-\epsilon_{ijk}\epsilon_{klm}\Omega_j\Omega_l x_m$ is the centripetal term and $-2\epsilon_{ijk}\Omega_j U_k$ is the Coriolis term, due to the rotating coordinate system. Because of the potential nature of the pressure, gravitational and centripetal terms, they are put together in what often is referred to as a *reduced* pressure gradient

$$-\frac{\partial P^*}{\partial x_i} = -\frac{\partial P}{\partial x_i} + \rho g_i - \rho\epsilon_{ijk}\epsilon_{klm}\Omega_j\Omega_l x_m$$

Thus, a relation for the *reduced* pressure is

$$P^* = P - \rho g_i x_i + \rho\epsilon_{ijk}\epsilon_{klm}\Omega_j\Omega_l x_m x_i$$

The star and the name '*reduced*' of P^* is omitted in the rest of this work and it is simply referred to as static pressure.

The boussinesq assumption for the Reynolds stress tensor $\overline{u_i' u_j'}$ reads

$$\rho\overline{u_i' u_j'} = -\mu_t\left(\frac{\partial U_i}{\partial x_j} + \frac{\partial U_j}{\partial x_i}\right) + \frac{2}{3}\delta_{ij}\rho k$$

where $k = \frac{1}{2}\overline{u_i' u_i'}$ is the turbulent kinetic energy. The $k - \omega$ model of Wilcox [11] for the turbulent kinetic energy k and the specific dissipation rate ω reads

$$\begin{aligned}
\frac{\partial \rho U_j k}{\partial x_j} &= \frac{\partial}{\partial x_j}\left[\left(\mu + \frac{\mu_t}{\sigma_k}\right)\frac{\partial k}{\partial x_j}\right] + P_k - \rho\beta^\star\omega k \\
\frac{\partial \rho U_j \omega}{\partial x_j} &= \frac{\partial}{\partial x_j}\left[\left(\mu + \frac{\mu_t}{\sigma_\omega}\right)\frac{\partial \omega}{\partial x_j}\right] + \frac{\omega}{k}\left(c_{\omega 1}P_k - c_{\omega 2}\rho k\omega\right)
\end{aligned}$$

where the turbulent viscosity μ_t is defined as

$$\mu_t = \rho\frac{k}{\omega}$$

The production term reads

$$P_k = \mu_t\left(\frac{\partial U_i}{\partial x_j} + \frac{\partial U_j}{\partial x_i}\right)\frac{\partial U_i}{\partial x_j} - \frac{2}{3}\rho k\frac{\partial U_i}{\partial x_i}$$

and the closure coefficients are defined from experiment as

$$\beta^\star = 0.09,\ c_{\omega 1} = \tfrac{5}{9},\ c_{\omega 2} = \tfrac{3}{40},\ \sigma_k = 2 \text{ and } \sigma_\omega = 2$$

2.3 Numerical considerations

The geometry is a four-blade and 24 guide-vane Kaplan turbine. If the spiral casing distributes the flow axisymmetrically (a good assumption according to the turbine manufacturer) it is reasonable to believe that the runner flow is periodic over an angle of 90 degrees. This assumption together with periodic boundary conditions reduces the computational domain to $1/4$th of its original size. The computational domain starts after the guide vanes, assuming axisymmetric flow defined by the guide vane angle and the volume flow. A fully developed turbulent $1/7$th velocity and turbulent kinetic energy inlet profile is assumed. The inlet turbulent lengtscale is prescribed so

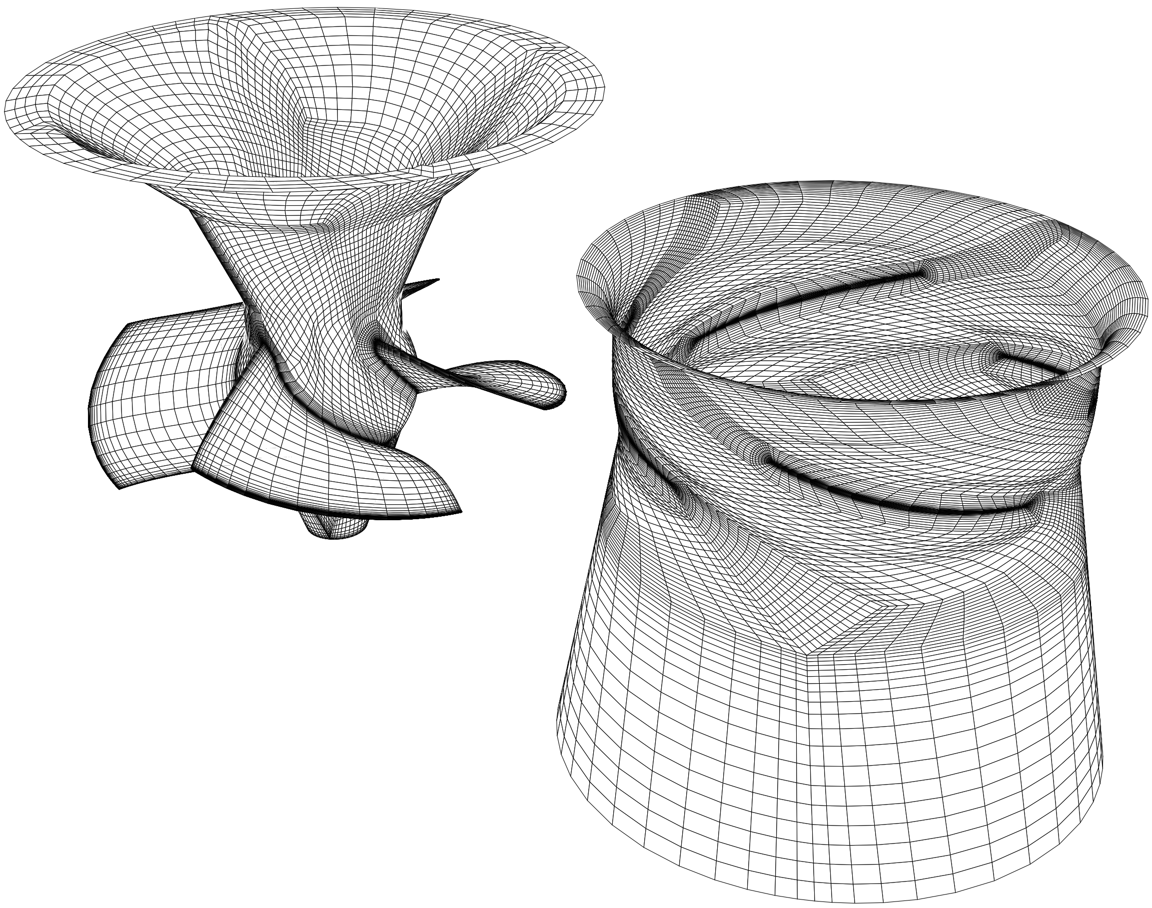

Figure 2.1: The surface grid. The runner and the shroud have been separated horizontally.

that a constant value of $\mu_t/\mu = 10$ (μ is the dynamic viscosity and μ_t is the turbulent viscosity from the turbulence model) is obtained across the inlet. The outlet is prescribed as a fully developed outlet ensuring global continuity during the computations [10].

Since the computational domain is rotating, Coriolis and centripetal effects are included in the momentum equations. At this stage, the $k - \omega$ model of Wilcox [11], which can be integrated all the way to the wall, is used without terms for rotational effects. This is common in turbomachinery computations for reasons of numerical stability and the small impact of such terms in these kinds of industrial applications [1, 2]. At the walls, no slip condition is assumed for the velocities and Low-Re turbulence boundary conditions [11] are assumed. A hybrid differencing scheme, which is second order accurate for diffusion and first order accurate for convection, is used.

2.4 Computational grid

The computational grid is visualized in figure 2.1, where only the grid lines attached to the surfaces are shown. Here, the resolution of all the boundary layers are visible. This grid contains 365 445 grid-points. The reasons for a complicated topology like this are several: The precision of the results depend on the orthogonality of the grid. Also, the grid should attach to the runner blade surfaces as orthogonal as possible. The multiblock solver is conformal (grid lines must be continous) on all block interfaces, including periodic boundaries. The resolution of boundary layers on hub, shroud and runner blade should not unnecessarily resolve other regions, in order to keep the grid size low and numerical convergence high. A single block conformal grid would meet none of the above demands. It would also be very complicated to include the tip clearance. The grid generation is definitely the most important and time consuming part of CFD in complex domains. Without a good grid, the models does not work and the solutions does not converge or produces inaccurate results.

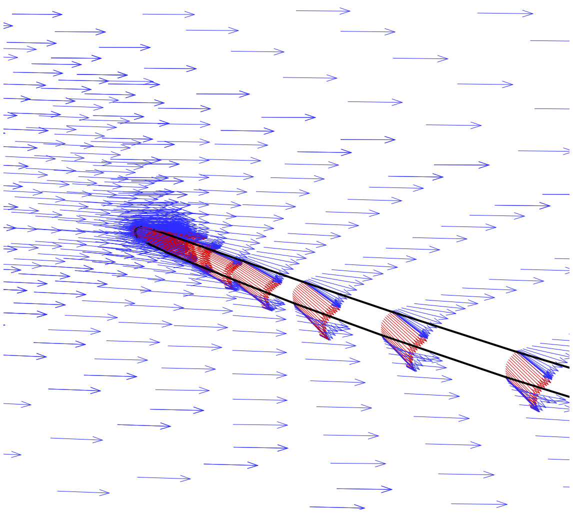

(a) Relative (rotating frame of reference) velocity vectors at a distance of $0.125mm$ from the shroud (at the center of the tip clearance). Note that this is inside the shroud boundary layer. The solid line indicates the leading edge tip runner blade profile.

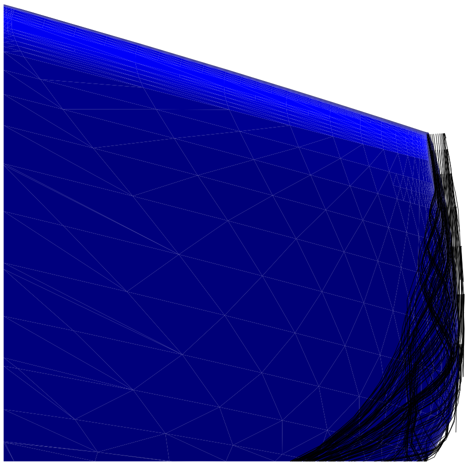

(b) Streamlines emitted from inside the tip clearance, close to the leading edge form a vortical structure. The leading edge suction side tip is shown in the figure.

Figure 3.1: Tip clearance velocity vectors and streamlines.

3 Results

There is reason to believe that the tip clearance flow produces a vortical structure due to separation (on the runner suction side) of the jet flow through the tip clearance (figure 3.1(a)) and its interaction with the shroud boundary layer. The most obvious proof for this comes from observations of tip clearance cavitational dynamics. Looking at high speed films of tip clearance cavitation, the cavitation bubbles seems to originate close to the leading edge [7]. They are then transported (in a rotating frame of reference) along the suction side of the tip clearance in a vortical structure. The flow in this region is highly unsteady. However, the mean steady flow should also reveal some vortical structure. Some vortical structure close to the leading edge tip clearance can be seen when emitting a large number of streamlines in this region of the computational results (figure 3.1(b)). Single streamlines rather quickly escapes from this structure. The problem with escaping streamlines may be due to numerical errors involved when computing them. Close to vortex cores small interpolation errors may easily make the streamline escape into the surroundings. The main differences between the flow in the studied cases is that the leading edge load and the tip cavitation (due to the tip clearance mass flow) increases when N_{11} decreases [9]. The following sections investigates these computed flow features.

3.1 Runner blade pressure distribution

To visualize the blade loading, the static pressure coefficient is extracted along a profile close to the tip of a runner blade (figure 3.2). In section 2.1 it was stated that the main difference between the flow in the four cases studied in this work is that the leading edge load should increase when N_{11} decrease (N_{11} is presented in table 2.1 for the different cases). This feature is captured by the calculations.

3.2 Tip clearance mass flow

The mass flow through the tip clearance and the part of the total mass flow that escapes through the tip clearance and thus does not contribute to the efficiency of the machine is displayed in table 3.1. The tip clearance mass flow decreases with decreasing N_{11}, but the the part of the total mass flow that escapes through the tip clearance increases. In figure 3.3, the relative (rotating frame of reference) velocity distribution through the tip clearance is displayed. These results are the radially averaged velocities at the vertical center of the tip clearance. It can clearly be seen that the main feature of the tip clearance flow is that the magnitude of the axial velocity is largest close to

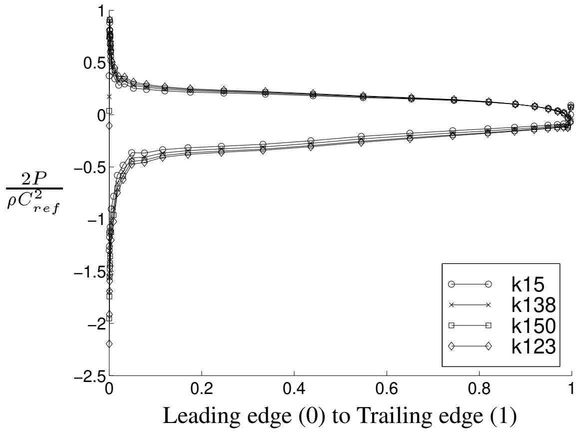

Figure 3.2: Runner blade static pressure coefficient distribution at a profile close to the tip of a runner blade. (Pressure normalized using the reference velocity $C_{ref} = \Omega D/2$, where Ω is the angular rotation.)

Case	k15	k138	k150	k123
$\dot{m}_{tip}$	$2.15 \cdot 10^{-4}$	$2.12 \cdot 10^{-4}$	$2.12 \cdot 10^{-4}$	$2.08 \cdot 10^{-4}$
$\dot{m}_{tip}/\dot{m}_{tot}$	$2.88 \cdot 10^{-3}$	$2.98 \cdot 10^{-3}$	$3.04 \cdot 10^{-3}$	$3.08 \cdot 10^{-3}$

Table 3.1: Tip clearance mass flow.

the leading edge of the tip clearance. These results are in accordance with the theories of a strong leading edge tip clearance jet, interacting with the suction side shroud boundary layer. This results in a leading edge tip vortex with low vortex core static pressure, causing cavitation. The tangential and axial components of the relative tip clearance velocity profiles of the different cases are compared in figure 3.4. The main differences between the four cases occur at the leading edge of the tip clearance, where the tangential component is reduced and the magnitude of the axial component increases with decreasing N_{11}. The increase of the magnitude of the axial component with decreased N_{11} is in accordance with the tip clearance cavitation pattern. The amount of tip clearance cavitation formation increases with decreasing N_{11} [9].

3.3 Validation

The CFD code CALC-BFC has been used and validated [10] in a large number of applications. The parallel domain decomposition of the code (CALC-PMB) has been validated in [10]. Future work will include validation of the code, specifically for water turbine applications. The problem with this kind of validation is the lack of detailed measurements to compare with.

4 Discussion

The purpose of the Swedish water turbine program is to increase the Swedish water power competence in order to meet the growing water power demand in Sweden together with the demands on environmental care and efficiency. It is believed that future CFD (Computational Fluid Dynamics) can be a complement to model testing, speeding up the design procedure. However, the introduction of CFD in production of water turbines cannot be done without experience of CFD comparable to experience of model testing in this field. This work has increased the experience of CFD in the water turbine field.

The main feature of the tip clearance flow results is that the magnitude of the axial velocity is very large close to the leading edge of the tip clearance. These results are in accordance with the theories of a strong leading edge tip clearance jet, interacting with the suction side shroud boundary layer. The magnitude of the axial component increases with decreasing N_{11}. This is in accordance with the tip clearance cavitation pattern. The amount of tip clearance cavitation formation increases with decreasing N_{11}.

The computational results shows that the tip blade loading increases when N_{11} decreases. This is in accordance with with the turbine manufacturer [9].

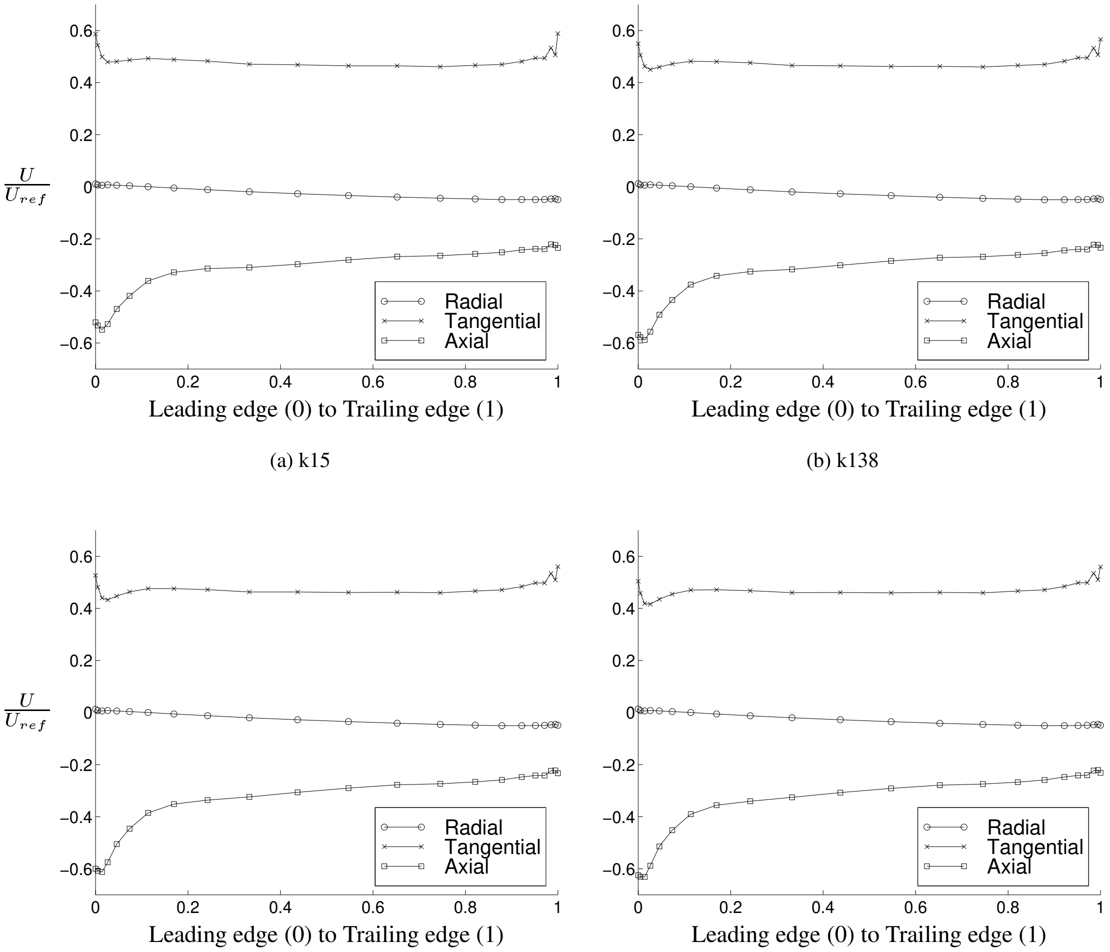

(a) k15

(b) k138

(c) k150

(d) k123

Figure 3.3: Tip clearance relative velocity profiles. (Relative velocity normalized using the reference velocity $U_{ref} = \Omega D/2$, where Ω is the angular rotation.)

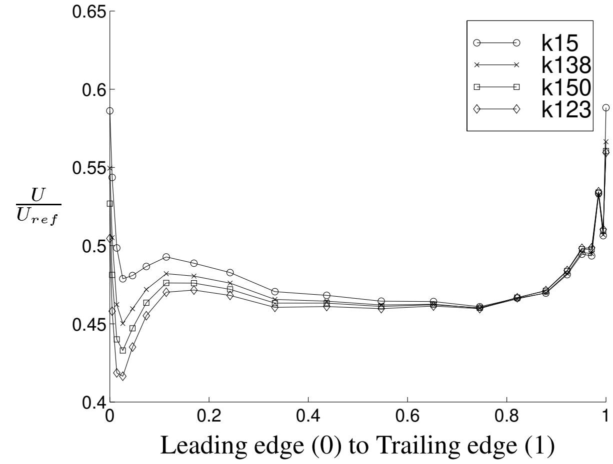

(a) Tangential

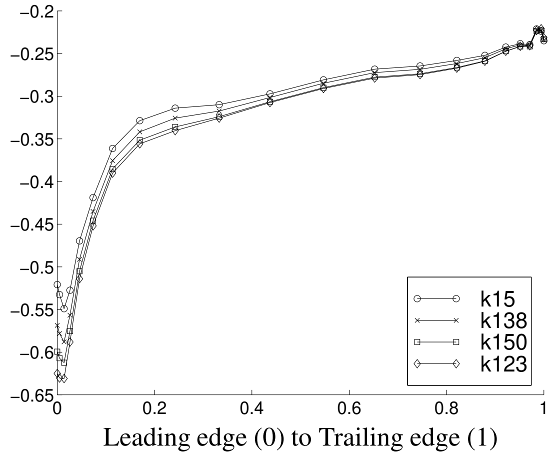

(b) Axial

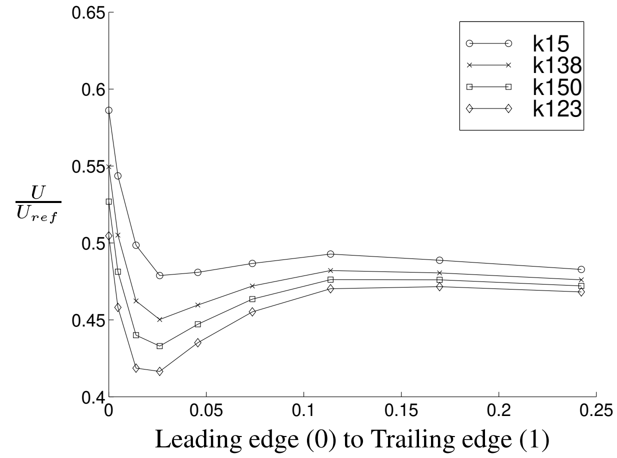

(c) Tangential (zoom)

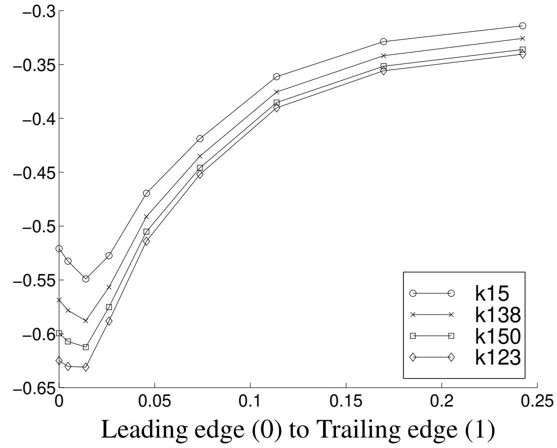

(d) Axial (zoom)

Figure 3.4: Tip clearance relative velocity profiles. (Relative velocity normalized using the reference velocity $U_{ref} = \Omega D/2$, where Ω is the angular rotation.)

It is necessary to perform both simulations and detailed measurements on the same geometry. The correct boundary conditions, from measurements, must be applied in the simulations and the results must be validated against measurements. This will be included in future work.

The grid generation is definitely the most important and time consuming part of CFD in complex domains. Without a good grid, the models does not work and the solutions does not converge or gives inaccurate results. In order to reduce grid generation time and optimize the grid quality, automatic grid generation templates for each water turbine type should be generated. This is especially important when comparing different runner blade angles.

The flow in water turbines is highly transient due to the guide vane wakes and the inherent instabilities downstream. Some of the features of the flow cannot be captured using Reynolds averaged methods. Using LES (Large Eddy Simulation), these features could be investigated. This will be included in future work.

References

[1] S. Baralon. Private communication. *Dept. of Thermo and Fluid Dynamics, Chalmers University of Technology*, 1998.

[2] J. Bredberg. Private communication. *Dept. of Thermo and Fluid Dynamics, Chalmers University of Technology*, 1999.

[3] S. Dahlström, H. Nilsson, and L. Davidson. Lesfoil: 6-months progress report by Chalmers. Technical report, Dept. of Thermo and Fluid Dynamics, Chalmers University of Technology, Gothenburg, 1998.

[4] L. Davidson. An introduction to turbulence models. Int.rep. 97/2, Thermo and Fluid Dynamics, Chalmers University of Technology, Gothenburg, 1997.

[5] L. Davidson and B. Farhanieh. CALC-BFC: A finite-volume code employing collocated variable arrangement and cartesian velocity components for computation of fluid flow and heat transfer in complex three-dimensional geometries. Rept. 92/4, Thermo and Fluid Dynamics, Chalmers University of Technology, Gothenburg, 1992.

[6] J.P. Van Doormaal and G.D. Raithby. Enhancements of the SIMPLE method for predicting incompressible fluid flows. *Num. Heat Transfer*, 7:147–163, 1984.

[7] M. Grekula. Private communication. *Dept. of Naval Architecture and Ocean Engineering, division of Hydromechanics, Chalmers University of Technology*, 1999.

[8] P.K. Kundu. *Fluid Mechanics*. Academic Press, San Diego, California, 1990.

[9] B. Nauclér. Private communication. *Kvaerner Turbin AB*, 1998.

[10] H. Nilsson and L. Davidson. CALC-PVM: A parallel SIMPLEC multiblock solver for turbulent flow in complex domains. Int.rep. 98/12, Thermo and Fluid Dynamics, Chalmers University of Technology, Gothenburg, 1998.

[11] D.C. Wilcox. Reassessment of the scale-determining equation for advanced turbulence models. *AIAA J.*, 26(11):1299–1310, 1988.

Biographical details of the authors

H. Nilsson graduated in Physical Oceanography from the University of Gothenburg in 1997. From 1997 he has been a Ph.D student at Chalmers University of Technology, Gothenburg, where he specializes in numerical simulation of turbulent flow in Kaplan water turbines using parallel super computers.

L. Davidson is a Professor of Heat Transfer at Chalmers University of Technology, Gothenburg, where he specializes in numerical turbulence modelling. He is the supervisor of H. Nilsson.